J. Fluid Mech. (2024), *vol*. 998, A2, doi:10.1017/jfm.2024.627

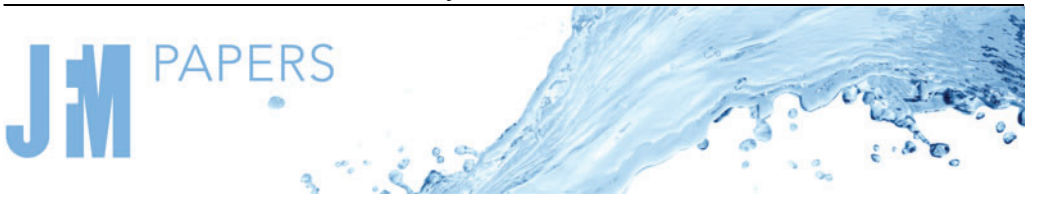

Swimming efficiency in viscosity gradients

Jiahao Gong[1], **Vaseem A. Shaik**[2] **and Gwynn J. Elfring**[1,2,†]

[1]Department of Mathematics, Institute of Applied Mathematics, University of British Columbia, Vancouver, BC V6T 1Z2, Canada

[2]Department of Mechanical Engineering, Institute of Applied Mathematics, University of British Columbia, Vancouver, BC V6T 1Z4, Canada

(Received 25 April 2024; revised 26 July 2024; accepted 29 July 2024)

In this note, we study the effect of viscosity gradients on the energy dissipated by the motion of microswimmers and the associated efficiency of that motion. Using spheroidal squirmer model swimmers in weak linearly varying viscosity fields, we find that efficiency depends on whether they generate propulsion from the back (pushers) or the front (pullers). Pushers are faster and more efficient when moving down gradients, but slower and less efficient moving up viscosity gradients, and the opposite is true for pullers. However, both pushers and pullers display negative viscotaxis, therefore pushers dynamically tend to the most efficient orientation, while pullers tend to the least. We also evaluate the effect of shape on power expenditure and efficiency when swimming in viscosity gradients, and find that in general, the change in both due to gradients decreases monotonically with increasing slenderness. This work shows how shape and gait play an important role in determining dynamics and efficiency in inhomogeneous environments, and demonstrating that both efficiency minimizing and maximizing stable dynamical states are possible.

Key words: micro-organism dynamics

1. Introduction

Swimming microorganisms are widely found in nature and are important in a diverse array of biological processes (Vogel 1996; Lauga 2016; Wadhwa & Berg 2022; Ishikawa & Pedley 2023*a*,*b*). An understanding of the dynamics of microswimmers and other active particles (biological or synthetic) in homogeneous Newtonian fluids is now reasonably well developed (Brennen & Winet 1977; Lauga & Powers 2009; Yeomans, Pushkin & Shum 2014; Elgeti, Winkler & Gompper 2015; Ishikawa 2024). However, natural environments can often be quite complex and inhomogeneous (Bechinger *et al.* 2016; Martínez-Calvo, Trenado-Yuste & Datta 2023).

† Email address for correspondence: gelfring@mech.ubc.ca

Inhomogeneity of fluid environments can arise due to spatial variations of different physical quantities, including light (Jékely 2009), heat (Bahat *et al.* 2003), chemical concentration and nutrients (Berg & Brown 1972; Berg 2004), and can lead to directed motion, which is known as taxis. Natural bodies of water, such as lakes, ponds and oceans, often have gradients in temperature or salinity, and these inhomogeneities can also lead to a stratification of the mechanical properties of the fluid such as density and viscosity (Stocker 2012). In response to gradients in viscosity, bacteria such as *Leptospira* and *Spiraplasma* have been observed to perform positive viscotaxis by swimming up the gradients (Kaiser & Doetsch 1975; Petrino & Doetsch 1978; Daniels, Longland & Gilbart 1980; Takabe *et al.* 2017), while *Escherichia coli* and *Chlamydomonas reinhardtii* perform negative viscotaxis by swimming down the gradients (Sherman, Timkina & Glagolev 1982; Coppola & Kantsler 2021; Stehnach *et al.* 2021). A gradient in the viscosity of the intestinal mucosal barrier is thought to control the spatial organization of intestinal microbiota (Swidsinski *et al.* 2007).

While there is an obvious benefit associated with moving to an environment where the energetic penalty of motion is lower, recent work has shown that such directed motion can arise as an immediate consequence of interaction with an environment with inhomogeneous mechanical properties. Inhomogeneity can break rotational symmetry, and this leads naturally to reorientation in order to conserve angular momentum. In pioneering work, Liebchen *et al.* (2018) showed that active particles, modelled as linked spheres moving with a constant propulsive force, in weak viscosity gradients exhibited positive viscotaxis due to the mismatch of viscous drag on the spheres. Further investigations incorporated the impact of viscosity changes on propulsion using the spherical (Datt & Elfring 2019; Shaik & Elfring 2021; Gong, Shaik & Elfring 2023) and spheroidal (Gong, Shaik & Elfring 2024) squirmer models, which simulates a swimming gait by a surface slip velocity. These studies found that the interaction between the particle's active slip and spatial variations of viscosity tends to dominate the dynamics and typically results in negative viscotaxis, although the effect of the gradient decreases with increased slenderness.

Changes in translational and rotational dynamics that arise as a consequence of viscosity gradients are now relatively well understood, for both passive (Kamal & Lauga 2023; Anand & Narsimhan 2024) and active (Gong *et al.* 2024) particles, but here we focus on the power expended by microswimmers and any associated changes in efficiency that are caused by the inhomogeneous environment. Even though some microswimmers are capable of achieving higher speeds in viscosity gradients, we still need to quantify the resultant changes in power expenditure in order to determine whether such motion is in fact more efficient. We assess the efficiency of microswimmers using the Froude efficiency, which is defined as the ratio of the power expended to simply drag a body of the same shape to the power expended by propulsion (Lighthill 1952). This efficiency has been used broadly to characterize different microswimmers in homogeneous Newtonian fluids (Stone & Samuel 1996; Chattopadhyay *et al.* 2006; Ishimoto & Gaffney 2014), although more recently, other efficiency measures have been proposed (Childress 2012; Nasouri, Vilfan & Golestanian 2021; Daddi-Moussa-Ider, Golestanian & Vilfan 2023), to guarantee a measure that can never exceed unity.

Several studies have investigated the efficiency of microswimmers in homogeneous non-Newtonian environments. One study showed that pusher-type spherical squirmers always expend more power and swim less efficiently than puller-type squirmers in second-order fluids (De Corato, Greco & Maffettone 2015). In fluids with shear-thinning properties, all types of two-mode spherical squirmers swim more slowly, expending less

power with higher efficiency (Nganguia, Pietrzyk & Pak 2017), but by introducing a third squirming mode, it is possible to design a microswimmer that can swim faster and more efficiently in shear-thinning fluids. Specifically for mechanically inhomogeneous fluids, a swimming sheet was shown to expend more power and move with reduced efficiency in a viscosity stratified fluid in comparison to a homogeneous Newtonian fluid (Dandekar & Ardekani 2020).

In this work, we aim to explore how viscosity gradients affect the swimming efficiency of spheroidal squirmers in order to understand the role of swimming gait and shape on power expended and efficiency in an inhomogeneous fluid. In what follows, we derive analytical formulas for the energy expended by these microswimmers and the associated efficiency assuming weak constant gradients in the viscosity.

2. Swimmers in viscosity gradients

2.1. *The squirmer model*

Microswimmers are modelled as squirmers in this research. The spherical squirmer model is a classical hydrodynamic model for the motion of self-propelling particles, such as protozoa or volvocine green algae, wherein the complex motions of ciliated surfaces are represented as a tangential slip velocity on the surface of a spherical body (Lighthill 1952; Blake 1971). The slip velocity is commonly written in terms of Legendre polynomials:

$$\boldsymbol{u}^s = -\sum_{n=1}^{\infty} \frac{2B_n}{n(n+1)} P_n'(\boldsymbol{p}\cdot\boldsymbol{n})\,\boldsymbol{p}\cdot(\boldsymbol{I}-\boldsymbol{nn}), \tag{2.1}$$

where $\boldsymbol{p}$ is the swimming direction of the particle, P_n is the Legendre polynomial of degree n, and $\boldsymbol{n}$ is a unit normal to the squirmer surface. The coefficients B_n, often called squirming modes, can be related to Stokes flow singularity solutions (Pak & Lauga 2014). The swimming velocity of a particle is determined by the B_1 mode (here, we assume $B_1 \geqslant 0$), while the B_2 mode sets the magnitude of the force dipole, the slowest decaying contribution to the far-field flow.

Since many organisms are elongated in shape, such as *Paramecium caudatum* or *Opalina*, the squirmer model was extended to accommodate spheroidal geometries by Keller & Wu (1977), and the streamlines predicted by their spheroidal model indeed closely matched the experimental streak photographs of *Paramecium caudatum*. The original model by Keller & Wu (1977) included only the first squirming mode, and latter studies added a force-dipole mode to better represent other types of microswimmers (Gaffney *et al.* 2011; Ishimoto & Gaffney 2014; Theers *et al.* 2016). We use the two-mode spheroidal squirmer here to represent prolate spheroidal active swimmers (Theers *et al.* 2016; van Gogh *et al.* 2022; Gong *et al.* 2024). The slip velocity on the surface of a prolate spheroidal squirmer can be expressed as

$$\boldsymbol{u}^s = -B_1(\boldsymbol{s}\cdot\boldsymbol{p})\,\boldsymbol{s} - \frac{B_2}{a}(\boldsymbol{r}\cdot\boldsymbol{p})(\boldsymbol{s}\cdot\boldsymbol{p})\boldsymbol{s}, \tag{2.2}$$

where $\boldsymbol{r}$ is a vector from the centre of the particle to a point on the surface, while $\boldsymbol{s}$ is the unit tangent at that point (see figure 1). This form is equivalent to the formula in (2.1) for a sphere with only two modes. Recent research points out that the swimming speed and stresslet of such a squirmer are influenced by more than just the B_1 and B_2 modes (Pöhnl, Popescu & Uspal 2020); however, these additional modes significantly affect the outcome only when the particle is notably slender. For most practical cases, the two-mode

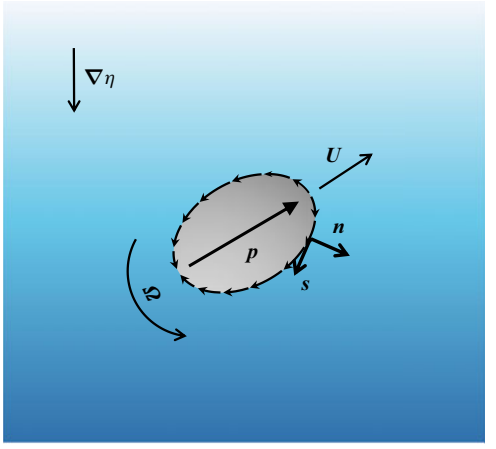

Figure 1. Schematic of a spheroidal squirmer swimming in a constant viscosity gradient $\nabla\eta$. Here, $\boldsymbol{p}$ represents the swimming direction of the swimmer.

prolate squirmer model (Theers *et al.* 2016; Qi *et al.* 2020; Chi *et al.* 2022; van Gogh *et al.* 2022; Gong *et al.* 2024) suffices to capture swimming dynamics. Thus identifying the coefficients B_1 and B_2 completely determines the swimming mechanism here.

It is common to define the squirming ratio $\beta = B_2/B_1$, in which case the sign of β determines whether the propulsion of the swimmer originates from its front or rear. Organisms like *Escherichia coli*, which generate propulsion from their rear, are classified as pushers and are characterized by $\beta < 0$. Conversely, organisms that draw fluid towards them from the front, such as *Chlamydomonas reinhardtii*, are known as pullers and are characterized by $\beta > 0$. There are also swimmers whose propulsion mechanisms are not predominantly directed from the front or the rear; one example is *Volvox carteri*, which has flagella evenly distributed across its spherical surface. For these organisms, referred to as neutral swimmers, $\beta = 0$.

2.2. *Newtonian fluid with viscosity gradients*

We endeavour to find the power expended by an active particle swimming in a Newtonian fluid with a spatially varying viscosity, and thereafter determine the efficiency of that motion. The active particle is modelled as a prolate spheroid. The spheroid is an axisymmetric ellipsoid with two equal-length equatorial semi-axes b and one longer polar semi-axis a ($b \leqslant a$). The eccentricity

$$e = \sqrt{1 - \frac{b^2}{a^2}} \tag{2.3}$$

represents the slenderness of the particle. When $e = 0$ ($b = a$), the particle is a sphere with radius a. The swimming direction $\boldsymbol{p}$ of the particle is the direction of its major axis.

Viscosity variations in fluids are caused by similar variations in temperature, salinity, nutrient or polymer concentrations that often occur over length scales much larger than the swimming microorganisms. For instance, the viscosity variations in microfluidic channels occur over 10^2–10^3 μm, while those in oceans, lakes and ponds occur over several metres to kilometres. Generally, it is reasonable to assume that viscosity varies linearly at the scale of small (μm-sized) organisms considered here, and indeed such local to particle

viscosity variations have been shown to largely capture changes in particle dynamics (Shaik & Elfring 2021). Moreover, one can also achieve close to linear viscosity profiles in microfluidic channels (Stehnach *et al.* 2021). Hence we consider a linearly varying viscosity field $\eta(\boldsymbol{x})$ varying over a large macroscopic length scale L such that

$$\boldsymbol{\nabla}\eta = \frac{\eta_\infty}{L}\,\boldsymbol{d}, \tag{2.4}$$

where η_∞ is the viscosity at an arbitrary point near the particle, and $\boldsymbol{d}$ is the unit direction of the viscosity gradient. Defining the dimensionless parameter $\epsilon = a/L \ll 1$ that characterizes the size of the particle vs the length scale of the gradient, we can write $\boldsymbol{\nabla}\eta = \epsilon(\eta_\infty/a)\boldsymbol{d}$.

The flow around the particle in a Newtonian fluid with a spatially varying viscosity at low Reynolds number is governed by the continuity equation and Cauchy's equation of motion:

$$\boldsymbol{\nabla}\cdot\boldsymbol{u} = 0, \tag{2.5}$$

$$\boldsymbol{\nabla}\cdot\boldsymbol{\sigma} = \boldsymbol{0}, \tag{2.6}$$

where $\boldsymbol{u}$ is the velocity field, and $\boldsymbol{\sigma} = -p\boldsymbol{I} + \eta(\boldsymbol{x})\,\dot{\boldsymbol{\gamma}}$ is the stress tensor. Here, p is the pressure, and $\dot{\boldsymbol{\gamma}} = \boldsymbol{\nabla}\boldsymbol{u} + (\boldsymbol{\nabla}\boldsymbol{u})^{\mathrm{T}}$ is twice the strain-rate tensor. Defining an extra stress

$$\boldsymbol{\tau}_{NN} = (\eta(\boldsymbol{x}) - \eta_\infty)\dot{\boldsymbol{\gamma}}, \tag{2.7}$$

we can alternatively write the stress tensor as

$$\boldsymbol{\sigma} = -p\boldsymbol{I} + \eta_\infty\dot{\boldsymbol{\gamma}} + \boldsymbol{\tau}_{NN}. \tag{2.8}$$

The boundary conditions on the flow field are that far away from the particle, the disturbance flow generated by the microswimmer should decay, which means that

$$\boldsymbol{u} \to \boldsymbol{0} \quad \text{as } |\boldsymbol{r}| \to \infty. \tag{2.9}$$

While on the particle surface (denoted by S_p), the fluid velocity $\boldsymbol{u}$ should satisfy no-slip conditions

$$\boldsymbol{u}(\boldsymbol{x} \in S_p) = \boldsymbol{U} + \boldsymbol{\Omega}\times\boldsymbol{r} + \boldsymbol{u}^s. \tag{2.10}$$

The slip velocity $\boldsymbol{u}^s$ is prescribed by (2.2), while the translational and rotational velocities, $\boldsymbol{U}$ and $\boldsymbol{\Omega}$, are determined by satisfying the additional constraints that since the microswimmers are considered as neutrally buoyant, there is no external force or torque acting on the particle, and in the absence of particle inertia, the hydrodynamic force and torque on the particle must both vanish:

$$\boldsymbol{F} = \int_{S_p} \boldsymbol{n}\cdot\boldsymbol{\sigma}\,\mathrm{d}S = \boldsymbol{0}, \tag{2.11}$$

$$\boldsymbol{L} = \int_{S_p} \boldsymbol{r}\times(\boldsymbol{n}\cdot\boldsymbol{\sigma})\,\mathrm{d}S = \boldsymbol{0}. \tag{2.12}$$

The power $\mathcal{P}$ expended by swimmer in its motion through the fluid is written as

$$\mathcal{P} = -\int_{S_p} \boldsymbol{n}\cdot\boldsymbol{\sigma}\cdot\boldsymbol{u}\,\mathrm{d}S = -\int_{S_p} \boldsymbol{n}\cdot\boldsymbol{\sigma}\cdot\boldsymbol{u}^s\,\mathrm{d}S, \tag{2.13}$$

where the latter form comes from substitution of the boundary conditions (2.10) and application of the force- and torque-free conditions. Alternatively, an application of the

divergence theorem yields the power expended by the swimmer in terms of the viscous dissipation in the fluid volume $\mathcal{V}$ in which the swimmer is immersed:

$$\mathcal{P} = \int_{\mathcal{V}} \boldsymbol{\sigma} : \nabla \boldsymbol{u} \, \mathrm{d}V = \frac{1}{2} \int_{\mathcal{V}} \eta(\boldsymbol{x}) \, \dot{\boldsymbol{\gamma}} : \dot{\boldsymbol{\gamma}} \, \mathrm{d}V. \tag{2.14}$$

Lighthill (1952) defined the efficiency $\mathcal{E}$ of a particle swimming at low Reynolds number as the ratio of the power $\hat{\mathcal{P}}$ required to simply drag the particle (as a rigid body) at the same velocity as it swims, to the power expended by swimming $\mathcal{P}$, in other words,

$$\mathcal{E} = \frac{\hat{\mathcal{P}}}{\mathcal{P}}. \tag{2.15}$$

The towing power $\hat{\mathcal{P}}$ in (2.15) is given by

$$\hat{\mathcal{P}} = -\hat{\boldsymbol{F}} \cdot \boldsymbol{U} - \hat{\boldsymbol{L}} \cdot \boldsymbol{\Omega}, \tag{2.16}$$

where the hydrodynamic force $\hat{\boldsymbol{F}}$ and torque $\hat{\boldsymbol{L}}$ due to undergoing the rigid-body motion with velocities $\boldsymbol{U}$ and $\boldsymbol{\Omega}$ can be written as

$$\begin{pmatrix} \hat{\boldsymbol{F}} \\ \hat{\boldsymbol{L}} \end{pmatrix} = - \begin{pmatrix} \boldsymbol{R}_{FU} & \boldsymbol{R}_{F\Omega} \\ \boldsymbol{R}_{LU} & \boldsymbol{R}_{L\Omega} \end{pmatrix} \cdot \begin{pmatrix} \boldsymbol{U} \\ \boldsymbol{\Omega} \end{pmatrix}, \tag{2.17}$$

where $(\boldsymbol{R}_{FU}, \boldsymbol{R}_{F\Omega}, \boldsymbol{R}_{LU}, \boldsymbol{R}_{L\Omega})$ are rigid-body resistance tensors dependent on the eccentricity e, the orientation vector $\boldsymbol{p}$, and the viscosity gradient $\nabla\eta$. The detailed expressions are given in Appendix B.

3. Asymptotic analysis

Since the gradient in viscosity is considered weak, as characterized by $\epsilon \ll 1$, we expand all flow terms $\{\boldsymbol{u}, \boldsymbol{\sigma}, \boldsymbol{\tau}_{NN}, \dot{\boldsymbol{\gamma}}, \mathcal{P}, \hat{\mathcal{P}}, \mathcal{E}\}$ assuming a regular perturbation expansion in ϵ, for example, $\boldsymbol{u} = \boldsymbol{u}_0 + \epsilon \boldsymbol{u}_1 + O(\epsilon^2)$.

The spatially varying viscosity field can be written in terms of the centre of the particle $\boldsymbol{x}_c$ as

$$\eta(\boldsymbol{x}) = \eta(\boldsymbol{x}_c) + (\boldsymbol{x} - \boldsymbol{x}_c) \cdot \nabla\eta = \eta(\boldsymbol{x}_c) + \epsilon \, \frac{\eta_\infty}{a} \, \boldsymbol{d} \cdot (\boldsymbol{x} - \boldsymbol{x}_c). \tag{3.1}$$

The centre of the particle need not necessarily be in the plane $\mathcal{X}_\infty$ where $\eta(\boldsymbol{x}) = \eta_\infty$, but we can always define η_∞ near the particle such that the distance $|\boldsymbol{d} \cdot (\boldsymbol{x} - \boldsymbol{x}_c)|/a \ll O(1/\epsilon)$ for $\boldsymbol{x} \in \mathcal{X}_\infty$, hence $\eta(\boldsymbol{x}_c) = \eta_\infty + O(\epsilon)$.

3.1. *Homogeneous fluids*

At leading order, $\epsilon \to 0$, the viscosity is homogeneous, so we simply have an active particle swimming in a Newtonian fluid with a constant viscosity. The corresponding flow field is well known, for both spherical and spheroidal active particles, and given in Appendix A. According to (2.14), the leading-order value of power dissipation has the

form

$$\mathcal{P}_0 = \frac{1}{2}\int_{\mathcal{V}} \eta_\infty \dot{\boldsymbol{\gamma}}_0 : \dot{\boldsymbol{\gamma}}_0 \,\mathrm{d}S. \tag{3.2}$$

Evaluating the integral, we obtain

$$\mathcal{P}_0 = \pi a \eta_\infty (\mathcal{A} + \mathcal{B}\beta^2) B_1^2, \tag{3.3}$$

where the terms $\mathcal{A}$ and $\mathcal{B}$ are functions of only the eccentricity and have the form

$$\mathcal{A} = \frac{2(1-e^2)[-2e + (1+e^2)\mathcal{L}_e]}{e^3}, \tag{3.4}$$

$$\mathcal{B} = \frac{-8e^2(45 - 51e^2 + 8e^4) + 24e(15 - 22e^2 + 7e^4)\mathcal{L}_e + 6(-15 + 27e^2 - 13e^4 + e^6)\mathcal{L}_e^2}{3e^5[6e + (-3 + e^2)\mathcal{L}_e]}, \tag{3.5}$$

$$\mathcal{L}_e = \ln((1+e)/(1-e)). \tag{3.6}$$

Keller & Wu (1977) derived the above result for a neutral spheroidal squirmer, but here we have added the contribution of the second mode to obtain a formula valid for pushers and pullers. When $e \to 0$, $\mathcal{A} = 16/3$ and $\mathcal{B} = 8/3$, and we obtain the result for a spherical squirmer derived by Lighthill (1952) and Blake (1971):

$$\mathcal{P}_{0,sphere} = \tfrac{8}{3}\pi(2+\beta^2)\eta_\infty a B_1^2 = 6\pi a \eta_\infty (2+\beta^2) U_{0,sphere}^2, \tag{3.7}$$

where $U_{0,sphere} = 2B_1/3$ is the swimming speed of a spherical squirmer in Newtonian fluid with uniform viscosity. Here, $\mathcal{A}$ and $\mathcal{B}$ are monotonically decreasing functions of eccentricity, meaning that power diminishes as a spheroidal squirmer becomes more slender, and when $e \to 1$, $\mathcal{A} = \mathcal{B} = 0$, meaning that an infinitely slender squirmer requires no power to move (with speed equal to B_1) through a homogeneous Newtonian fluid.

The efficiency at leading order is

$$\mathcal{E}_0 = \frac{\hat{\mathcal{P}}_0}{\mathcal{P}_0} = \frac{\boldsymbol{U}_0 \cdot \boldsymbol{R}_{FU}^{(0)} \cdot \boldsymbol{U}_0 + \boldsymbol{\Omega}_0 \cdot \boldsymbol{R}_{L\Omega}^{(0)} \cdot \boldsymbol{\Omega}_0}{\mathcal{P}_0}. \tag{3.8}$$

Using classic results of the rigid-body resistance (see Appendix B) and the velocity of a spheroidal squirmer in a homogeneous Newtonian fluid (Keller & Wu 1977),

$$\boldsymbol{U}_0 = \frac{2e - (1-e^2)\mathcal{L}_e}{2e^3} B_1 \boldsymbol{p}, \tag{3.9}$$

$$\boldsymbol{\Omega}_0 = \boldsymbol{0}, \tag{3.10}$$

we obtain the efficiency

$$\mathcal{E}_0 = \frac{\mathcal{F}}{\mathcal{A} + \mathcal{B}\beta^2}, \tag{3.11}$$

where

$$\mathcal{F} = \frac{4[2e + (-1+e^2)\mathcal{L}_e]^2}{e^3[-2e + (1+e^2)\mathcal{L}_e]} \tag{3.12}$$

is a monotonically decreasing function of slenderness e. When $e \to 0$, $\mathcal{F} = 8/3$ and we obtain the classic efficiency of a two-mode spherical squirmer,

$$\mathcal{E}_{0,sphere} = \frac{1}{2+\beta^2}. \tag{3.13}$$

In the slender limit, $\mathcal{E}_0(e \to 1) = 3/\beta^2$, meaning that efficiency is finite given the presence of the wasteful B_2 mode.

3.2. *Effect of gradients*

The effect of viscosity variations on the power dissipation in (2.14) are captured at $O(\epsilon)$ by

$$\epsilon\,\mathcal{P}_1 = \frac{1}{2}\int_{\mathcal{V}} (\eta(\boldsymbol{x}) - \eta_\infty)\dot{\boldsymbol{\gamma}}_0 : \dot{\boldsymbol{\gamma}}_0 \,\mathrm{d}V. \tag{3.14}$$

Terms involving $\dot{\boldsymbol{\gamma}}_1$ are identically zero due to the force- and torque-free condition (De Corato *et al.* 2015; Nganguia *et al.* 2017), so power at this order involves only integrating the leading-order homogeneous flow field. Similarly, the particle dynamics in viscosity gradients can be written as an integral of the leading-order flow field, although against a different kernel (Gong *et al.* 2024), hence as the efficiency depends on power and particle dynamics, it can also be found from the leading-order homogeneous flow field. With the above formula, we obtain the power dissipation, valid up to $O(\epsilon)$:

$$\mathcal{P} = \pi(\mathcal{A} + \mathcal{B}\beta^2)\,\eta(\boldsymbol{x}_c)\,aB_1^2 + \pi a^2 \mathcal{C} B_1^2 \beta(\boldsymbol{p}\cdot\nabla\eta), \tag{3.15}$$

where

$$\mathcal{C} = \frac{4(-1+e^2)[6e + (-3+e^2)\mathcal{L}_e]}{e^5} \tag{3.16}$$

is a monotonically decreasing function of eccentricity. Taking the limit $e \to 0$, $\mathcal{C} = 32/15$ and we obtain for a sphere that

$$\mathcal{P}_{sphere} = \frac{8}{3}\pi(2+\beta^2)\,\eta(\boldsymbol{x}_c)\,aB_1^2 + \frac{32}{15}\pi a^2 B_1^2 \beta(\boldsymbol{p}\cdot\nabla\eta). \tag{3.17}$$

What we see is that pushers ($\beta < 0$) require less power to swim up viscosity gradients, and more to swim down viscosity gradients, in comparison to a homogeneous fluid, while the opposite is true for pullers ($\beta > 0$). Neutral squirmers ($\beta = 0$) do not see a change in power. The reason for this change in power expended can be understood in terms of the change in speed experienced by the squirmers. Previous research (Datt & Elfring 2019; Gong *et al.* 2024) showed that pushers generate more thrust and thus swim faster and dissipate more energy when moving down viscosity gradients; conversely, they generate less thrust, swim slower and dissipate less energy when moving up viscosity gradients. The opposite is true for pullers.

A spheroidal squirmer always dissipates less power (for the same B_1 and B_2 values) as $\mathcal{A}$, $\mathcal{B}$ and $\mathcal{C}$ are all monotonically decreasing functions of the slenderness e, that all go to zero when $e \to 1$.

The correction to the efficiency, at $O(\epsilon)$, can be written as

$$\mathcal{E}_1 = \frac{\hat{\mathcal{P}}_1}{\mathcal{P}_0} - \mathcal{E}_0 \frac{\mathcal{P}_1}{\mathcal{P}_0}. \tag{3.18}$$

From Appendix B, we know that $\boldsymbol{R_{FU}}$, $\boldsymbol{R_{L\Omega}}$ are $O(1)$ at the leading order, while $\boldsymbol{R_{F\Omega}}$, $\boldsymbol{R_{LU}}$ are $O(\epsilon)$ as a result:

$$\hat{\mathcal{P}}_1 = 2\boldsymbol{U}_1 \cdot \boldsymbol{R}_{\boldsymbol{FU}}^{(0)} \cdot \boldsymbol{U}_0 + \boldsymbol{U}_0 \cdot \boldsymbol{R}_{\boldsymbol{FU}}^{(1)} \cdot \boldsymbol{U}_0. \tag{3.19}$$

The correction to particle velocities due to viscosity variations, $\boldsymbol{U}_1$ and $\boldsymbol{\Omega}_1$, are from Gong *et al.* (2024):

$$\boldsymbol{U}_1 = -\frac{B_2}{5} (\mathcal{X}^U \boldsymbol{I} - \mathcal{Y}^U 3\boldsymbol{pp}) \cdot \boldsymbol{d}, \tag{3.20}$$

$$\boldsymbol{\Omega}_1 = -\frac{1}{2a} \mathcal{X}^{\Omega} \boldsymbol{U}_0 \times \boldsymbol{d}, \tag{3.21}$$

where

$$\mathcal{X}^U = \frac{5[-6e + 4e^3 + 3(1-e^2)\mathcal{L}_e][-6e + 10e^3 + 3(1-e^2)^2\mathcal{L}_e]}{24e^5[6e - (3-e^2)\mathcal{L}_e]}, \tag{3.22}$$

$$\mathcal{Y}^U = \frac{5[-6e + 4e^3 + 3(1-e^2)\mathcal{L}_e][-18e + 6e^3 + (9 - 6e^2 + 5e^4)\mathcal{L}_e]}{72e^5[6e - (3-e^2)]}, \tag{3.23}$$

$$\mathcal{X}^{\Omega} = \frac{(1-e^2)[-2e + (1+e^2)\mathcal{L}_e]}{(2-e^2)[2e - (1-e^2)\mathcal{L}_e]}. \tag{3.24}$$

However, note that $\boldsymbol{\Omega}_1$ is not needed for $\hat{\mathcal{P}}_1$. Substituting $\hat{\mathcal{P}}_1$ and $\mathcal{P}_1$ from (3.15) into (3.18), we can calculate the efficiency valid to $O(\epsilon)$ as

$$\mathcal{E} = \frac{\mathcal{F}}{\mathcal{A} + \mathcal{B}\beta^2} + \epsilon \frac{\mathcal{G} + \mathcal{H}\beta^2}{(\mathcal{A} + \mathcal{B}\beta^2)^2} \beta(\boldsymbol{p} \cdot \boldsymbol{d}), \tag{3.25}$$

where $\mathcal{G}$ (for $e < 0.964$) and $\mathcal{H}$ are monotonically decreasing function of slenderness:

$$\begin{aligned}\mathcal{G} = {} & 8(1-e^2)[2e + (-1+e^2)\mathcal{L}_e][8e^3(45 + 3e^2 + 2e^4) - 4e^2(135 - 84e^2 + 5e^4 + 4e^6)\mathcal{L}_e \\ & + 2e(135 - 177e^2 + 51e^4 + 5e^6 + 2e^8)\mathcal{L}_e^2 - 3(1-e^2)^2(15 + e^4)\mathcal{L}_e^3] \\ & \times \{3e^8[6e + (-3+e^2)\mathcal{L}_e][-2e + (1+e^2)\mathcal{L}_e]\}^{-1},\end{aligned} \tag{3.26}$$

$$\begin{aligned}\mathcal{H} = {} & 4[2e + (-1+e^2)\mathcal{L}_e] \\ & \times [8e^2(45 - 51e^2 + 8e^4) - 24e(15 - 22e^2 + 7e^4)\mathcal{L}_e \\ & - 6(-15 + 27e^2 - 13e^4 + e^6)\mathcal{L}_e^2] \\ & \times [4e^2(-9 + 3e^2 + 2e^4) - 4e(-9 + 6e^2 + e^6)\mathcal{L}_e + 3(-3 + 3e^2 - e^4 + e^6)\mathcal{L}_e^2] \\ & \times \{9e^{10}[6e + (-3+e^2)\mathcal{L}_e]^2[-2e + (1+e^2)\mathcal{L}_e]\}^{-1}.\end{aligned} \tag{3.27}$$

For spheres, $e \to 0$, the efficiency simplifies to

$$\mathcal{E}_{sphere} = \frac{1}{2 + \beta^2} + \epsilon \frac{8 + 6\beta^2}{5(2 + \beta^2)^2} \beta(\boldsymbol{p} \cdot \boldsymbol{d}). \tag{3.28}$$

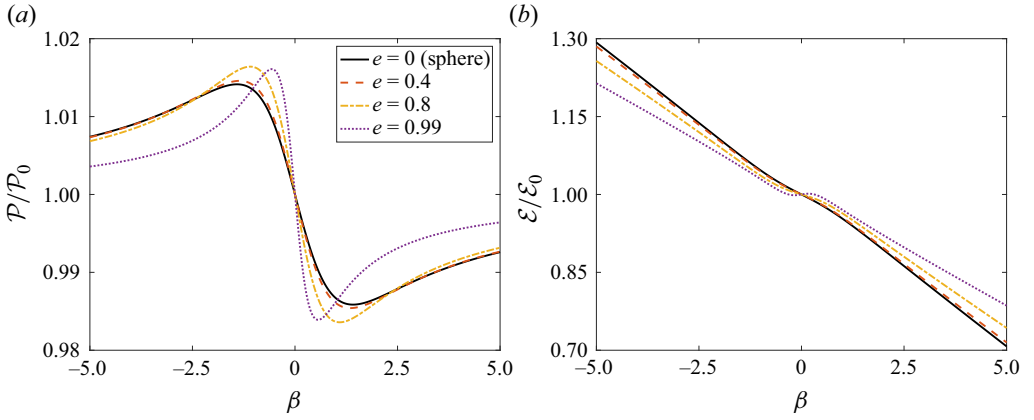

Figure 2. Variation of (*a*) relative power expenditure and (*b*) swimming efficiency of a swimmer moving down viscosity gradients with squirming ratio β and eccentricity e. Power expenditure is evaluated by choosing the viscosity at the centre of the swimmer as η_∞ ($\eta(\boldsymbol{x}_c) = \eta_\infty$).

The essential message of these formulas is that, similar to speed and power, the correction to efficiency due to viscosity gradients is proportional to $\beta(\boldsymbol{p}\cdot\boldsymbol{d})$, meaning that, for example, when swimming down viscosity gradients, pushers are faster and expend more power, but are more efficient, while pullers are slower, expend less power and are less efficient. These trends are illustrated in figure 2, which shows the variation of relative power and efficiency as a function of β for various eccentricities e. The opposite is true when swimming up viscosity gradients; however, we know that swimming up viscosity gradients is dynamically unstable, and all squirmers tend to perform negative viscotaxis.

In deriving these formulas, we have assumed that the background viscosity remains fixed even in the presence of the particle. However, variations in viscosity generally arise from variations in an underlying field that affects the viscosity, such as temperature, salt or nutrient concentration, and taking into account the effect of boundary conditions on the surface of the particle in relation to the underlying field will then lead to changes in the viscosity. In Appendix C, we determine the effects of imposing a 'no-flux' condition for viscosity at the surface of the particle, and the associated effects on power expended and efficiency. Although there are quantitative differences in the parameters, the qualitative picture described above remains unchanged.

We have also neglected the higher-order ($n > 2$) squirming modes. The higher-order modes do not affect the velocity of a spherical squirmer in a homogeneous fluid (Lighthill 1952; Blake 1971) or in viscosity gradients (Datt & Elfring 2019; Shaik & Elfring 2021). But they do affect the velocity of a spheroidal squirmer in homogeneous fluids (Pöhnl *et al.* 2020), and we expect the effect to persist even in viscosity gradients. However, higher-order modes affect power dissipation and swimming efficiency in all cases, regardless of the presence of viscosity gradients or swimmer shape. In Appendix D, we give general formulas for power dissipation and efficiency for arbitrary spherical squirmers, and from those equations, we see that the effect of higher-order modes generally diminishes rapidly with the mode number n, and so may often be reasonably neglected. However, the presence of additional modes can substantially change the picture depending on the magnitude of the higher modes. For example, a three-mode pusher swimming down the viscosity gradients can dissipate more or less power and swim more or less efficiently as compared to in homogeneous fluids. We expect these broad insights on the effect

of higher-order modes for a spherical squirmer to translate qualitatively to a spheroidal squirmer.

4. Conclusion

In this work, we derived analytical formulas for the power expended by spheroidal squirmers swimming in linearly varying viscosity fields, and the associated efficiency of that motion. We found that pushers are faster and more efficient when moving down gradients, but slower and less efficient moving up viscosity gradients, and the opposite is true for pullers. We also evaluated the effect of shape on power expenditure and efficiency when swimming in viscosity gradients, and found that the change in both due to gradients diminishes monotonically with increasing slenderness.

Swimming down viscosity gradients is favourable for pushers because they generate thrust from the rear, where the viscosity is highest, which leads to faster swimming and thus a greater level of power expenditure; however, the energetic cost of this boost is lower (relative to rigid body motion) in comparison to a homogeneous fluid, thus the increase in efficiency. While both pushers and pullers can minimize or maximize efficiency depending on orientation relative to the gradient, both display negative viscotaxis, which means that pushers dynamically tend to the most efficient orientation while pullers tend to the least. However, this conclusion is sensitive to geometry. For example, if we construct a pusher made from a very thin 'tail' that generates thrust, and a large head that bears the majority of the drag, then this sort of swimmer would display positive viscotaxis (Gong *et al.* 2024), and be efficiency minimizing. This shows how shape and gait play a critical role in driving dynamics in inhomogeneous environments, and how both efficiency minimizing and maximizing dynamical states can be stable depending on the specific shape and gait. This raises questions about whether organisms might adjust their swimming gait in light of this fact. Finally, we note that while a puller is less efficient moving down a viscosity gradient in comparison to a homogeneous fluid of the same viscosity, it will still be energetically preferable to move to the region of lower viscosity, even if the instantaneous dynamics is slower and less efficient.

Funding. This work was supported by the Natural Sciences and Engineering Research Council of Canada (RGPIN-2020-04850) and by a UBC Killam Accelerator Research Fellowship to G.J.E.

Declaration of interests. The authors report no conflict of interest.

Author ORCIDs.
Vaseem A. Shaik https://orcid.org/0000-0002-7011-9176;
Gwynn J. Elfring https://orcid.org/0000-0002-9602-7261.

Appendix A. An active prolate spheroid in Stokes flow

The flow field $\boldsymbol{u}_0$ of an active spheroid swimming in a Newtonian fluid with uniform viscosity can be expressed in terms of a stream function ψ_0 (Keller & Wu 1977; Theers *et al.* 2016; van Gogh *et al.* 2022) as

$$\boldsymbol{u}_0 = \frac{1}{c^2\sqrt{\zeta_1^2-\zeta_2^2}}\left(\frac{1}{\sqrt{\zeta_1^2-1}}\frac{\partial\psi_0}{\partial\zeta_2}\boldsymbol{e}_{\zeta_1} - \frac{1}{\sqrt{1-\zeta_2^2}}\frac{\partial\psi_0}{\partial\zeta_1}\boldsymbol{e}_{\zeta_2}\right), \tag{A1}$$

using prolate spheroid coordinates $O'\zeta_1\zeta_2\phi$, where O' is the centre of the spheroid at $\boldsymbol{x}_c$. The spheroidal coordinate system can be related to a particle-aligned Cartesian coordinate

system $O'X_1X_2X_3$ as follows:

$$\left.\begin{aligned} X_1 &= c\sqrt{\zeta_1^2-1}\sqrt{1-\zeta_2^2}\cos\phi,\\ X_2 &= c\sqrt{\zeta_1^2-1}\sqrt{1-\zeta_2^2}\sin\phi,\\ X_3 &= c\zeta_1\zeta_2, \end{aligned}\right\} \tag{A2}$$

where $1 \leqslant \zeta_1 < \infty$, $-1 \leqslant \zeta_2 \leqslant 1$ and $0 \leqslant \phi < 2\pi$. Here, $c = \sqrt{a^2-b^2}$ is half of the focal length. We can define $\tilde{\zeta_1} = 1/e$, with $\zeta_1 > \tilde{\zeta}_1$ corresponding to the fluid domain exterior to the surface $\zeta_1 = \tilde{\zeta}_1$ of the particle.

The stream function ψ_0 has the solution

$$\begin{aligned} \psi_0 = {} & C_1 H_2(\zeta_1) G_2(\zeta_2) + C_2\zeta_1(1-\zeta_2^2)\\ & + C_3 H_3(\zeta_1) G_3(\zeta_2) + C_4\zeta_2(1-\zeta_2^2) + \tfrac{1}{2}U_0c^2(\zeta_1^2-1)(1-\zeta_2^2). \end{aligned} \tag{A3}$$

Here, $H_n(x)$ and $G_n(x)$ are Gegenbauer functions of the first and second order of degree $-1/2$ (Theers *et al.* 2016). The coefficients C_n are

$$\left.\begin{aligned} C_1 &= 2c^2\,\frac{U_0(\tilde{\zeta}_1^2+1) - 2B_1\tilde{\zeta}_1^2}{-\tilde{\zeta}_1 + (1+\tilde{\zeta}_1^2)\coth^{-1}\tilde{\zeta}_1},\\ C_2 &= c^2\,\frac{B_1\tilde{\zeta}_1[\tilde{\zeta}_1 - (\tilde{\zeta}_1^2-1)\coth^{-1}\tilde{\zeta}_1 - U_0]}{-\tilde{\zeta}_1 + (1+\tilde{\zeta}_1^2)\coth^{-1}\tilde{\zeta}_1},\\ C_3 &= c^2\,\frac{4B_2\tilde{\zeta}_1}{3\tilde{\zeta}_1 + (1-3\tilde{\zeta}_1^2)\coth^{-1}\tilde{\zeta}_1},\\ C_4 &= c^2\,\frac{B_2\tilde{\zeta}_1[2/3 - \tilde{\zeta}_1^2 + \tilde{\zeta}_1(\tilde{\zeta}_1^2-1)\coth^{-1}\tilde{\zeta}_1]}{3\tilde{\zeta}_1 + (1-3\tilde{\zeta}_1^2)\coth^{-1}\tilde{\zeta}_1}, \end{aligned}\right\} \tag{A4}$$

and $U_0 = |\boldsymbol{U}_0|$ is given in (3.9).

Appendix B. Resistance tensor for a passive prolate spheroid in viscosity gradient

Here, we derive the resistance tensor for a spheroidal particle undergoing rigid-body motion in a fluid with a linearly varying viscosity field. We follow steps similar to those shown in a previous paper deriving the mobility of a spheroidal particle in a viscosity gradient (Gong *et al.* 2024), and likewise, we use compact six-dimensional vectors for velocities $\boldsymbol{U} = (\boldsymbol{U}, \boldsymbol{\Omega})^{\mathrm{T}}$ and forces and torques $\hat{\boldsymbol{F}} = (\hat{\boldsymbol{F}}, \hat{\boldsymbol{L}})^{\mathrm{T}}$ to simplify formulas. Following the notation of this paper, the hat notation corresponds to values associated with rigid-body motion.

The resistance tensor to leading order, $\boldsymbol{R}_{\boldsymbol{FU}}^{(0)}$, corresponding to a homogeneous fluid with uniform viscosity η_∞, is well known and given by Kim & Karilla (1991).

The hydrodynamic force and torque in a viscosity gradient can be written as

$$\hat{\boldsymbol{F}} = -\boldsymbol{R}_{\boldsymbol{FU}}^{(0)} \cdot \boldsymbol{U} + \hat{\boldsymbol{F}}_{NN}. \tag{B1}$$

The 'extra' hydrodynamic force and torque corresponding to the extra stress $\hat{\boldsymbol{\tau}}_{NN}$ from the gradient can be shown, by the reciprocal theorem, to be

$$\hat{\boldsymbol{F}}_{NN} = -\int_{\mathcal{V}} \hat{\boldsymbol{\tau}}_{NN} : \hat{\boldsymbol{E}}_{\boldsymbol{U}}^{(0)} \,\mathrm{d}V, \tag{B2}$$

where the operator $\hat{\boldsymbol{E}}_{\boldsymbol{U}}^{(0)}$ corresponds to the rate of strain tensor in a homogeneous fluid,

$$\hat{\dot{\boldsymbol{\gamma}}}_0 = 2\hat{\boldsymbol{E}}_{\boldsymbol{U}}^{(0)} \cdot \boldsymbol{U}, \tag{B3}$$

and may be calculated with the flow field due to a spheroid undergoing rigid-body motion in a homogeneous Newtonian fluid, given by Kim & Karilla (1991). Substituting $\hat{\boldsymbol{\tau}}_{NN} = (\eta(\boldsymbol{x}) - \eta_\infty)\widehat{\dot{\boldsymbol{\gamma}}}$ into the equation above, and expanding terms in powers of ϵ, we obtain

$$\hat{\boldsymbol{F}}_{NN} = -\int_{\mathcal{V}} 2(\eta(\boldsymbol{x}) - \eta_\infty)\hat{\boldsymbol{E}}_{\boldsymbol{U}}^{(0)} : \hat{\boldsymbol{E}}_{\boldsymbol{U}}^{(0)} \cdot \boldsymbol{U} \,\mathrm{d}V + O(\epsilon^2), \tag{B4}$$

hence we can identify

$$\epsilon \boldsymbol{R}_{\boldsymbol{FU}}^{(1)} = \int_{\mathcal{V}} 2(\eta(\boldsymbol{x}) - \eta_\infty)\hat{\boldsymbol{E}}_{\boldsymbol{U}}^{(0)} : \hat{\boldsymbol{E}}_{\boldsymbol{U}}^{(0)} \,\mathrm{d}V. \tag{B5}$$

Combining terms, the resistance tensor accurate to $O(\epsilon)$ is $\boldsymbol{R}_{\boldsymbol{FU}} = \boldsymbol{R}_{\boldsymbol{FU}}^{(0)} + \epsilon \boldsymbol{R}_{\boldsymbol{FU}}^{(1)}$, where

$$\boldsymbol{R}_{\boldsymbol{FU}} = \begin{pmatrix} \boldsymbol{R}_{FU} & \boldsymbol{R}_{F\Omega} \\ \boldsymbol{R}_{LU} & \boldsymbol{R}_{L\Omega} \end{pmatrix}, \tag{B6}$$

and $\boldsymbol{R}_{F\Omega} = \boldsymbol{R}_{LU}^{\mathrm{T}}$. The resistance depends on the eccentricity e, the orientation vector $\boldsymbol{p}$, and the viscosity gradient $\nabla\eta$. Detailed expressions for all couplings in (B6) are

$$\boldsymbol{R}_{FU} = 6\pi\,\eta(\boldsymbol{x}_c)\,a[\mathcal{X}^A \boldsymbol{pp} + \mathcal{Y}^A(\boldsymbol{I} - \boldsymbol{pp})], \tag{B7}$$

$$\boldsymbol{R}_{L\Omega} = 8\pi\,\eta(\boldsymbol{x}_c)\,a^3[\mathcal{X}^C \boldsymbol{pp} + \mathcal{Y}^C(\boldsymbol{I} - \boldsymbol{pp})], \tag{B8}$$

$$\boldsymbol{R}_{F\Omega} = \boldsymbol{R}_{LU}^{\top} = \epsilon 6\pi\eta_\infty a^2[\lambda_1(\boldsymbol{d} \times \boldsymbol{I}) + \lambda_2(\boldsymbol{p} \cdot \boldsymbol{d})(\boldsymbol{p} \times \boldsymbol{I}) + \lambda_3 \boldsymbol{p}(\boldsymbol{d} \times \boldsymbol{p})], \tag{B9}$$

where

$$\lambda_1 = \frac{16e^3(1-e^2)}{9[-2e+(1-3e^2)\mathcal{L}_e]}, \tag{B10}$$

$$\lambda_2 = \frac{8[6e^4(1-e^2)+e^3(-3+4e^2+3e^4)\mathcal{L}_e]}{9[-2e+(1+e^2)\mathcal{L}_e][-2e+(1-3e^2)\mathcal{L}_e]}, \tag{B11}$$

$$\lambda_3 = \frac{4[e^5(36-28e^2)+e^4(-36+40e^2+4e^4)\mathcal{L}_e+e^3(9-13e^2-e^4+5e^6)\mathcal{L}_e^2]}{9[-2e+(1+e^2)\mathcal{L}_e]^2[-2e+(1-3e^2)\mathcal{L}_e]}, \tag{B12}$$

$$\mathcal{X}^A = \frac{8e^3}{3[-2e+(1+e^2)\mathcal{L}_e]}, \tag{B13}$$

$$\mathcal{Y}^A = \frac{16e^3}{3[2e+(3e^2-1)\mathcal{L}_e]}, \tag{B14}$$

$$\mathcal{X}^C = \frac{4e^3(1-e^2)}{3[2e-(1-e^2)\mathcal{L}_e]}, \tag{B15}$$

$$\mathcal{Y}^C = \frac{4e^3(2-e^2)}{3[-2e+(1+e^2)\mathcal{L}_e]} \tag{B16}$$

are functions of eccentricity e.

Appendix C. Disturbance viscosity effects

Variations in viscosity generally arise from variations in an underlying field that affects the viscosity, such as temperature, salt or nutrient concentration. Taking into account the effect of boundary conditions on the surface of the particle in relation to the underlying field will then lead to changes in the viscosity. For example, in an otherwise linear salt concentration field, the presence of a particle will disrupt the field due to salt impermeability. Although these disturbances diminish with distance from the particle, the disturbance does have a leading-order effect on the dynamics of the active particle (Shaik & Elfring 2021).

Here, we determine the power dissipation and swimming efficiency, factoring in the disturbance to viscosity due to the application of a no-flux condition at the particle's surface. The total viscosity field can be represented as the superposition of an ambient viscosity field (denoted as η_0) and a disturbance viscosity field (denoted by a prime):

$$\eta = \eta_0 + \eta'. \tag{C1}$$

The boundary conditions on the disturbance viscosity field η' are that the disturbance viscosity should diminish in the far-field region:

$$\eta' \to 0 \quad \text{as } |\boldsymbol{r}| \to \infty. \tag{C2}$$

The transport of scalar fields, such as temperature, salt or nutrient concentrations, can be characterized using an advection–diffusion equation. When variations in these scalar fields are minimal, changes in viscosity can be modelled with a similar advection–diffusion equation. For slow-moving microswimmers in environments with highly diffusive scalar fields, such as temperature or salt concentration, advection is minimal, resulting in the

viscosity distribution following the Laplace equation. Since the ambient viscosity field is linear, the disturbance viscosity field must also conform to the Laplace equation,

$$\nabla^2\eta = \nabla^2\eta' = 0. \tag{C3}$$

The disturbance viscosity field is also governed by the boundary conditions on the particle's surface. We consider the surface to be impermeable to salt or insulated against temperature changes, and this leads to an associated 'no-flux' condition for viscosity at the particle's boundary,

$$\boldsymbol{n}\cdot\nabla\eta = 0 \quad \text{on } S_p. \tag{C4}$$

Supposing that the ambient viscosity field is along $\boldsymbol{e}_1$, the mathematical expression of the disturbance viscosity field η' in a particle-aligned coordinate is

$$\eta' = A_{1,0}\, P_1^0(\zeta_2)\, Q_1^0(\zeta_1) + A_{1,1}\, P_1^1(\zeta_2)\, Q_1^1(\zeta_1)\cos(\phi), \tag{C5}$$

where

$$A_{1,0} = \epsilon\eta_\infty p_1 \frac{2e(1-e^2)}{[2e-(1-e^2)\mathcal{L}_e]}, \tag{C6}$$

$$A_{1,1} = \epsilon\eta_\infty\sqrt{1-p_1^2}\,\frac{2e(1-e^2)}{[2e-4e^3-(1-e^2)\mathcal{L}_e]}. \tag{C7}$$

Here, $p_1 = \boldsymbol{p}\cdot\boldsymbol{e}_1$, and P_k^m and Q_k^m denote the associated Legendre polynomials of the first and second kinds, with degree k and order m. Their detailed mathematical formulations can be found in Abramowitz & Stegun (1964).

The power dissipation of a prolate spheroidal squirmer with a no-flux condition is, to first order,

$$\mathcal{P} = \pi(\mathcal{A}+\mathcal{B}\beta^2)\,\eta(\boldsymbol{x}_c)\,aB_1^2 + \pi a^2\mathcal{C}^{nf}B_1^2\beta(\boldsymbol{p}\cdot\nabla\eta), \tag{C8}$$

where

$$\mathcal{C}^{nf} = \frac{8(-1+e^2)[6e+(-3+e^2)\mathcal{L}_e]}{e^2[2e+(-1+e^2)\mathcal{L}_e]} \tag{C9}$$

is a monotonically decreasing function of eccentricity. For a sphere, $e\to 0$, $\mathcal{C}^{nf} = 16/5$, and we have

$$\mathcal{P}^{nf}_{sphere} = \tfrac{8}{3}\pi(2+\beta^2)\,\eta(\boldsymbol{x}_c)\,aB_1^2 + \tfrac{16}{5}\pi a^2B_1^2\beta(\boldsymbol{p}\cdot\nabla\eta). \tag{C10}$$

The corresponding swimming efficiency up to $O(\epsilon)$ is

$$\mathcal{E} = \frac{\mathcal{F}}{\mathcal{A}+\mathcal{B}\beta^2} + \epsilon\,\frac{\mathcal{G}^{nf}+\mathcal{H}^{nf}\beta^2}{(\mathcal{A}+\mathcal{B}\beta^2)^2}\,\beta(\boldsymbol{p}\cdot\boldsymbol{d}), \tag{C11}$$

where

$$\begin{aligned}\mathcal{G}^{nf} = {}& 8(1-e^2)[8e^3(45+87e^2-32e^4)+4e^2(-135-36e^2+19e^4+32e^6)\mathcal{L}_e\\ &+(270e-426e^3+402e^5-182e^7)\mathcal{L}_e^2+(-45+186e^2-212e^4+54e^6+17e^8)\mathcal{L}_e^3\\ &-12e(1-e^2)^2(1+e^2)\mathcal{L}_e^4]\times\{3e^5[6e+(-3+e^2)\mathcal{L}_e][-2e+(1+e^2)\mathcal{L}_e]\}^{-1},\end{aligned} \tag{C12}$$

$$\mathcal{H}^{nf} = 8[-4e^2(45-51e^2+8e^4)+12e(15-22e^2+7e^4)\mathcal{L}_e-3(15-27e^2+13e^4-e^6)\mathcal{L}_e^2] \times [4e^2(63-87e^2+32e^4)-4e(63-96e^2+37e^4)\mathcal{L}_e+(63-81e^2+e^4+17e^6)\mathcal{L}_e^2 - 12e(1-e^2)^2\mathcal{L}_e^3] \times \{9e^7[6e+(-3+e^2)\mathcal{L}_e]^2[-2e+(1+e^2)\mathcal{L}_e]\}^{-1}. \quad \text{(C13)}$$

Here, $\mathcal{G}^{nf}$ (for $e < 0.954$) and $\mathcal{H}^{nf}$ are monotonically decreasing functions of slenderness, and they both vanish when $e \to 1$. For a sphere, we obtain

$$\mathcal{E}^{nf}_{sphere} = \frac{1}{2+\beta^2} + \epsilon\,\frac{14+13\beta^2}{10(2+\beta^2)^2}\,\beta(\boldsymbol{p}\cdot\boldsymbol{d}). \quad \text{(C14)}$$

We see that taking into account the disturbance viscosity due to a no-flux boundary condition does not change the qualitative picture when compared to the effects of ambient viscosity alone.

Appendix D. Higher-order modes

A spherical squirmer with an arbitrary number of squirming modes B_n expends power

$$\mathcal{P}_{sphere} = \left(\frac{16}{3}B_1^2 + \sum_{n=2}^{\infty}\frac{16}{n(n+1)}B_n^2\right)\pi\,\eta(\boldsymbol{x}_c)\,a + \left(\frac{32}{15}B_1B_2 + \sum_{n=2}^{\infty}\frac{32}{(n+1)(2n+1)}B_nB_{n+1}\right)\pi a^2(\boldsymbol{p}\cdot\nabla\eta), \quad \text{(D1)}$$

and swims with efficiency

$$\mathcal{E}_{sphere} = \frac{B_1^2}{2B_1^2+\sum_{n=2}^{\infty}\frac{6}{n(n+1)}B_n^2} + \epsilon(\boldsymbol{p}\cdot\boldsymbol{d})\,\frac{\frac{8}{5}B_1^3B_2+\sum_{n=2}^{\infty}\left(\frac{36}{5n(n+2)}B_1B_2B_n^2-\frac{12}{(n+1)(2n+1)}B_1^2B_nB_{n+1}\right)}{\left(2B_1^2+\sum_{n=2}^{\infty}\frac{6}{n(n+1)}B_n^2\right)^2}. \quad \text{(D2)}$$

References

Abramowitz, M. & Stegun, I.A. 1964 *Handbook of Mathematical Functions with Formulas, Graphs, and Mathematical Tables*. Dover.

Anand, V. & Narsimhan, V. 2024 Sedimentation of spheroids in Newtonian fluids with spatially varying viscosity. *J. Fluid Mech.* **983**, A28.

Bahat, A., Tur-Kaspa, I., Gakamsky, A., Giojalas, L.C., Breitbart, H. & Eisenbach, M. 2003 Thermotaxis of mammalian sperm cells: a potential navigation mechanism in the female genital tract. *Nat. Med.* **9**, 149–150.

Bechinger, C., Di Leonardo, R., Löwen, H., Reichhardt, C., Volpe, G. & Volpe, G. 2016 Active particles in complex and crowded environments. *Rev. Mod. Phys.* **88**, 045006.

Berg, H.C. 2004 *E. coli in Motion*. Springer.

BERG, H.C. & BROWN, D.A. 1972 Chemotaxis in *Escherichia coli* analysed by three-dimensional tracking. *Nature* **239**, 500–504.

BLAKE, J.R. 1971 A spherical envelope approach to ciliary propulsion. *J. Fluid Mech.* **46**, 199–208.

BRENNEN, C. & WINET, H. 1977 Fluid mechanics of propulsion by cilia and flagella. *Annu. Rev. Fluid Mech.* **9**, 339–398.

CHATTOPADHYAY, S., MOLDOVAN, R., YEUNG, C. & WU, X.L. 2006 Swimming efficiency of bacterium *Escherichia coli*. *Proc. Natl Acad. Sci.* **103**, 13712–13717.

CHI, H., GAVRIKOV, A., BERLYAND, L. & ARANSON, I.S. 2022 Interaction of microswimmers in viscoelastic liquid crystals. *Commun. Phys.* **5**, 274.

CHILDRESS, S. 2012 A thermodynamic efficiency for Stokesian swimming. *J. Fluid Mech.* **705**, 77–97.

COPPOLA, S. & KANTSLER, V. 2021 Green algae scatter off sharp viscosity gradients. *Sci. Rep.* **11**, 399.

DADDI-MOUSSA-IDER, A., GOLESTANIAN, R. & VILFAN, A. 2023 Minimum entropy production by microswimmers with internal dissipation. *Nat. Commun.* **14**, 6060.

DANDEKAR, R. & ARDEKANI, A.M. 2020 Swimming sheet in a viscosity-stratified fluid. *J. Fluid Mech.* **895**, R2.

DANIELS, M.J., LONGLAND, J.M. & GILBART, J. 1980 Aspects of motility and chemotaxis in spiroplasmas. *Microbiology* **118**, 429–436.

DATT, C. & ELFRING, G.J. 2019 Active particles in viscosity gradients. *Phys. Rev. Lett.* **123**, 158006.

DE CORATO, M., GRECO, F. & MAFFETTONE, P.L. 2015 Locomotion of a microorganism in weakly viscoelastic liquids. *Phys. Rev.* E **92**, 053008.

ELGETI, J., WINKLER, R.G. & GOMPPER, G. 2015 Physics of microswimmers – single particle motion and collective behavior: a review. *Rep. Prog. Phys.* **78**, 056601.

GAFFNEY, E.A., GADÊLHA, H., SMITH, D.J., BLAKE, J.R. & KIRKMAN-BROWN, J.C. 2011 Mammalian sperm motility: observation and theory. *Annu. Rev. Fluid Mech.* **43**, 501–528.

VAN GOGH, B., DEMIR, E., PALANIAPPAN, D. & PAK, O.S. 2022 The effect of particle geometry on squirming through a shear-thinning fluid. *J. Fluid Mech.* **938**, A3.

GONG, J., SHAIK, V.A. & ELFRING, G.J. 2023 Active particles crossing sharp viscosity gradients. *Sci. Rep.* **13**, 596.

GONG, J., SHAIK, V.A. & ELFRING, G.J. 2024 Active spheroids in viscosity gradients. *J. Fluid Mech.* **984**, A26.

ISHIKAWA, T. 2024 Fluid dynamics of squirmers and ciliated microorganisms. *Annu. Rev. Fluid Mech.* **56**, 119–145.

ISHIKAWA, T. & PEDLEY, T.J. 2023*a* 50-year history and perspective on biomechanics of swimming microorganisms. Part I. Individual behaviours. *J. Biomech.* **158**, 111706.

ISHIKAWA, T. & PEDLEY, T.J. 2023*b* 50-year history and perspective on biomechanics of swimming microorganisms. Part II. Collective behaviours. *J. Biomech.* **160**, 111802.

ISHIMOTO, K. & GAFFNEY, E.A. 2014 Swimming efficiency of spherical squirmers: beyond the Lighthill theory. *Phys. Rev.* E **90**, 012704.

JÉKELY, G. 2009 Evolution of phototaxis. *Phil. Trans. R. Soc. Lond.* B*, Biol. Sci.* **364**, 2795–2808.

KAISER, G.E. & DOETSCH, R.N. 1975 Enhanced translational motion of *Leptospira* in viscous environments. *Nature* **255**, 656–657.

KAMAL, C. & LAUGA, E. 2023 Resistive-force theory of slender bodies in viscosity gradients. *J. Fluid Mech.* **963**, A24.

KELLER, S.R. & WU, T.Y. 1977 A porous prolate-spheroidal model for ciliated micro-organisms. *J. Fluid Mech.* **80**, 259–278.

KIM, S. & KARILLA, S.J. 1991 *Microhydrodynamics: Principles and Selected Applications*. Butterworth-Heinemann.

LAUGA, E. 2016 Bacterial hydrodynamics. *Annu. Rev. Fluid Mech.* **48**, 105–130.

LAUGA, E. & POWERS, T.R. 2009 The hydrodynamics of swimming microorganisms. *Rep. Prog. Phys.* **72**, 096601.

LIEBCHEN, B., MONDERKAMP, P., TEN HAGEN, B. & LÖWEN, H. 2018 Viscotaxis: microswimmer navigation in viscosity gradients. *Phys. Rev. Lett.* **120**, 208002.

LIGHTHILL, M.J. 1952 On the squirming motion of nearly spherical deformable bodies through liquids at very small Reynolds numbers. *Commun. Pure Appl. Math.* **5**, 109–118.

MARTÍNEZ-CALVO, A., TRENADO-YUSTE, C. & DATTA, S.S. 2023 Active transport in complex environments. In *Out-of-Equilibrium Soft Matter* (ed. C. Kurzthaler, L. Gentile & H.A. Stone), pp. 151–218. The Royal Society of Chemistry.

NASOURI, B., VILFAN, A. & GOLESTANIAN, R. 2021 Minimum dissipation theorem for microswimmers. *Phys. Rev. Lett.* **126**, 034503.

NGANGUIA, H., PIETRZYK, K. & PAK, O.S. 2017 Swimming efficiency in a shear-thinning fluid. *Phys. Rev.* E **96**, 062606.

PAK, O.S. & LAUGA, E. 2014 Generalized squirming motion of a sphere. *J. Engng Maths* **88**, 1–28.

PETRINO, M.G. & DOETSCH, R.N. 1978 'Viscotaxis', a new behavioural response of *Leptospira interrogans* (*biflexa*) strain B16. *J. Gen. Microbiol.* **109**, 113–117.

PÖHNL, R., POPESCU, M.N. & USPAL, W.E. 2020 Axisymmetric spheroidal squirmers and self-diffusiophoretic particles. *J. Phys. Condens. Matter* **32**, 164001.

QI, K., ANNEPU, H., GOMPPER, G. & WINKLER, R.G. 2020 Rheotaxis of spheroidal squirmers in microchannel flow: interplay of shape, hydrodynamics, active stress, and thermal fluctuations. *Phys. Rev. Res.* **2**, 033275.

SHAIK, V.A. & ELFRING, G.J. 2021 Hydrodynamics of active particles in viscosity gradients. *Phys. Rev. Fluids* **6**, 103103.

SHERMAN, M.Y., TIMKINA, E.O. & GLAGOLEV, A.N. 1982 Viscosity taxis in *Escherichia coli*. *FEMS Microbiol. Lett.* **13**, 137–140.

STEHNACH, M.R., WAISBORD, N., WALKAMA, D.M. & GUASTO, J.S. 2021 Viscophobic turning dictates microalgae transport in viscosity gradients. *Nat. Phys.* **17**, 926–930.

STOCKER, R. 2012 Marine microbes see a sea of gradients. *Science* **338**, 628–633.

STONE, H.A. & SAMUEL, A.D.T. 1996 Propulsion of microorganisms by surface distortions. *Phys. Rev. Lett.* **77**, 4102–4104.

SWIDSINSKI, A., SYDORA, B.C., DOERFFEL, Y., LOENING-BAUCKE, V., VANEECHOUTTE, M., LUPICKI, M., SCHOLZE, J., LOCHS, H. & DIELEMAN, L.A. 2007 Viscosity gradient within the mucus layer determines the mucosal barrier function and the spatial organization of the intestinal microbiota. *Inflamm. Bowel Dis.* **13**, 963–970.

TAKABE, K., TAHARA, H., ISLAM, M.S., AFFROZE, S., KUDO, S. & NAKAMURA, S. 2017 Viscosity-dependent variations in the cell shape and swimming manner of *Leptospira*. *Microbiology* **163**, 153–160.

THEERS, M., WESTPHAL, E., GOMPPER, G. & WINKLER, R.G. 2016 Modeling a spheroidal microswimmer and cooperative swimming in a narrow slit. *Soft Matter* **12**, 7372–7385.

VOGEL, S. 1996 *Life in Moving Fluids: The Physical Biology of Flow*. Princeton University Press.

WADHWA, N. & BERG, H.C. 2022 Bacterial motility: machinery and mechanisms. *Nat. Rev. Microbiol.* **20**, 161–173.

YEOMANS, J.M., PUSHKIN, D.O. & SHUM, H. 2014 An introduction to the hydrodynamics of swimming microorganisms. *Eur. Phys. J. Spec. Top.* **223** (9), 1771–1785.